

Biochemical and Functional Analysis of Smallpox Growth Factor (SPGF) and Anti-SPGF Monoclonal Antibodies*[§]

Received for publication, January 13, 2004, and in revised form, March 9, 2004
Published, JBC Papers in Press, April 7, 2004, DOI 10.1074/jbc.M400343200

Mikyung Kim^{‡§}, Hailin Yang^{‡§}, Sung-Kwon Kim^{¶¶}, Pedro A. Reche^{‡§}, Rebecca S. Tirabassi[¶],
Rebecca E. Hussey[‡], Yasmin Chishti[‡], James G. Rheinwald^{||}, Tiara J. Morehead^{**}, Tobias Zech[‡],
Inger K. Damon^{**}, Raymond M. Welsh[¶], and Ellis L. Reinherz[‡] ^{‡‡}

From the [‡]Laboratory of Immunobiology, Department of Medical Oncology, Dana-Farber Cancer Institute and Department of Medicine, Harvard Medical School, Boston, Massachusetts 02115, [¶]Department of Pathology, University of Massachusetts Medical Center, Worcester, Massachusetts 01655, ^{||}Department of Dermatology, Brigham and Women's Hospital, Harvard Medical School, Boston, Massachusetts 02115, and ^{**}Poxvirus Section, Centers for Disease Control and Prevention, Atlanta, Georgia 30333

Variola, the causative agent of smallpox, is a highly infectious double-stranded DNA virus of the orthopox genus that replicates within the cytoplasm of infected cells. For unknown reasons prominent skin manifestations, including “pox,” mark the course of this systemic human disease. Here we characterized smallpox growth factor (SPGF), a protein containing an epidermal growth factor (EGF)-like domain that is conserved among orthopox viral genomes, and investigated its possible mechanistic link. We show that after recombinant expression, refolding, and purification, the EGF domain of SPGF binds exclusively to the broadly expressed cellular receptor, erb-B1 (EGF receptor), with subnanomolar affinity, stimulating the growth of primary human keratinocytes and fibroblasts. High affinity monoclonal antibodies specific for SPGF reveal *in vivo* immunoprotection in a murine vaccinia pneumonia model by a mechanism distinct from viral neutralization. These findings suggest that blockade of pathogenic factor actions, in general, may be advantageous to the infected host.

Before its eradication, smallpox was a devastating disease afflicting humans for greater than 3000 years with significant morbidity and mortality (1). Variola virus enters through the respiratory tract, and human-human transmission usually occurs via large respiratory droplets. The asymptomatic, non-infectious incubation period averages 10–12 days (range 7–19 days) followed by fever, headache, and backache with a subsequent rash appearing on the face, trunk, and extremities and progressing to vesicles, pustules, and scabs lasting for several weeks. This rather lengthy incubation period provides time for naive, unvaccinated individuals to receive protective immunotherapy.

Large scale immunization with vaccinia virus (VV)¹ largely eliminated smallpox in Europe and North America by 1940. Subsequently, in 1967 the World Health Organization launched an intensified worldwide vaccination campaign resulting in eradication of smallpox by 1980 and cessation of vaccination (1). Given the susceptibility of unvaccinated individuals, the perceived potential for smallpox to be exploited as a mortality-inducing bioweapon is significant. In addition, immunization with VV is considered risky in immunocompromised or immunosuppressed individuals. However, advances in both immunology and genomic analysis may offer new possibilities for eliciting immune protection without the requirement for live-virus vaccination and attendant complications (2).

Viruses have evolved mechanisms to evade detection and destruction by the host immune system. One of the evasion strategies that has been adopted by large DNA viruses such as poxviruses and herpesviruses is to encode homologues of cytokines and chemokines and their receptors involved in immune modulation (3, 4). In the present report we employed genome-wide bioinformatic analysis to identify potential immune-accessible targets from variola virus for purposes of immunoprotection. Functional annotation indicated that one candidate protein, D4R, which is conserved among all *Orthopoxvirus*, corresponds to the variola virus counterpart of the vaccinia growth factor precursor (5). Vaccinia growth factor (VGF) is an early gene product involved in vaccinia pathogenesis. Host cell proliferative responses to vaccinia virus are mediated by VGF, and not surprisingly, deletion of the VGF factor gene reduces virus virulence *in vivo* (6, 7). Structurally, VGF is a highly glycosylated soluble factor related to the epidermal growth factor (EGF) superfamily, whose signature feature is the presence of an EGF-like domain (5, 8). Signaling by EGF-like ligands is mediated via four cell surface erb-B receptor kinases. Erb-B1, the epidermal growth factor receptor (EGFR), as well as erb-B2, -B3, and -B4 and their ligands have been studied in detail (for review, see Ref. 9). Poxviruses, including vaccinia, exploit the erb-B signaling network via their EGF-like growth factors (10).

* This work was supported by National Institutes of Health Grants AI50900 and AI19807 and a grant from the Dana Foundation (to E. L. R.) and National Institutes of Health Grant AR-35506 (to R. M. W.). The costs of publication of this article were defrayed in part by the payment of page charges. This article must therefore be hereby marked “advertisement” in accordance with 18 U.S.C. Section 1734 solely to indicate this fact.

[§] The on-line version of this article (available at <http://www.jbc.org>) contains Supplemental Figs. 1 and 2.

[‡] Equal contributors.

^{‡‡} To whom correspondence should be addressed: Dana-Farber Cancer Institute, 44 Binney St., Boston, MA 02115. Tel.: 617-632-3412; Fax: 617-632-3351; E-mail: ellis_reinherz@dfci.harvard.edu.

¹ The abbreviations used are: VV, vaccinia virus; EGFR, epidermal growth factor (EGF) receptor; IMV, intracellular mature virus; IFN γ , interferon γ ; mAb, monoclonal antibody; SPGF, smallpox growth factor; VGF, vaccinia growth factor; PBS, phosphate-buffered saline; HRPO, horseradish peroxidase; BSA, bovine serum albumin; FACS, fluorescence-activated cell sorter; MFI, mean fluorescence intensity; TGF, transforming growth factor; pfu, plaque-forming units; IL, interleukin; EEV, extracellular enveloped virus; EPI, epiregulin; ELISA, enzyme-linked immunosorbent assay; PDB, Protein Data Bank.

Thus, given the connection between viral pathogenesis and the expression of these EGF-like growth factors, we have isolated the smallpox growth factor (SPGF) from variola virus encoded by the D4R gene and expressed and purified the relevant recombinant fragment for functional studies, defining the human cellular target of SPGF. Monoclonal antibodies against this pathogenic factor were produced. Those with sufficiently high affinity and cross-reactive with the structurally related VGF were tested in a murine vaccine pneumonia *in vivo* model. The results suggest that blockade of viral secreted factors promoting pathogenesis may be advantageous for the infected host in general.

EXPERIMENTAL PROCEDURES

Protein Expression and Purification—Recombinant protein fragments of SPGF (D4R) and VGF (C11R) (residues 40–90) were constructed by PCR and subcloned into the pET15b vector using NdeI and BamHI restriction sites. In the resulting plasmid protein was expressed under the control of the T7 promoter as a fusion with a His₆ tag followed by a thrombin cleavage sequence at the N terminus. Protein was induced in *Escherichia coli* with isopropyl-1-thio- β -D-galactopyranoside at an A₆₀₀ of about 0.6 and harvested after 3 h of induction. The inclusion bodies were isolated and dissolved in 10 mM Tris, pH 8, containing 6 M guanidine HCl and 10 mM 2-mercaptoethanol. After oxidation overnight at room temperature, the protein was purified using a Ni²⁺-nitrilotriacetic acid-agarose column. The partially purified protein was diluted to 100 μ g/ml with 4 M guanidine HCl and dialyzed extensively at 4 °C against a 50 mM Tris, pH 9, buffer containing 50 mM NaCl, 2 mM reduced glutathione, and 1 mM oxidized glutathione. After three buffer exchanges over a 72-h period, during which oxidative refolding occurs, the refolded protein was buffer-exchanged to 20 mM sodium phosphate, pH 6.5, and 100 mM NaCl. Using a preparative C18 reverse-phase column, more than 90% of the refolded protein separated as a single sharp peak. Electrospray analysis on a mass spectrometer (Qstar Pulsar I) gave mass values of 7907 and 7870 Da for SPGF and VGF, respectively, consistent with their theoretical masses.

Chemical Cross-linking of SPGF and erb-B Receptors— 2.25×10^6 MB468 or MB453 cells were pretreated with 0.04% NaN₃ at 4 °C for 30 min to inhibit receptor internalization. Then biotinylated SPGF at 1 μ g/ml was incubated with the cells for 30 min at 4 °C. The dishes were washed with ice-cold Dulbecco's modified Eagle's medium. Bis(sulfosuccinimidyl) suberate (BS³) cross-linker was added to 1 mM and incubated for an additional 1 h at 4 °C with occasional shaking. After 2 washes with ice-cold PBS, 1 ml of lysis buffer (25 mM Tris, pH 7.4, 150 mM NaCl, 1% Triton X-100, 1 mM phenylmethylsulfonyl fluoride, 0.35 trypsin inhibitor units/ml aprotinin, and 5 μ g/ml leupeptin) was added directly to the dishes followed by shaking at 4 °C for 30 min. Samples were spun down, and the supernatants were subjected to immunoprecipitation with 1 μ g of anti-erb-B1, anti-erb-B3, or anti-erb-B4 (Santa Cruz) goat polyclonal antibodies or a 1:40 dilution of anti-erb-B2 (Cell Signaling) rabbit polyclonal antibody using 10 μ l of GammaBind™ plus beads. After rotating at 4 °C for 5 h, the beads were washed 4 times with 1 \times Tris-buffered saline, 1% Triton X-100 followed by boiling the beads directly in 2 \times SDS loading buffer. SDS-PAGE and Western blotting by streptavidin-HRP were used to reveal the biotinylated erb-B receptors.

For analysis of erb-B receptor subtype-specific expression in MB468 and MB453 cells, lysates as above were immunoprecipitated with the anti-erbB antisera and then Western-blotted with the same antibodies used for immunoprecipitation in the case of erb-B1 and erb-B3 and goat anti-erb-B2 polyclonal antibody (Cell Signaling Technology Inc.) and rabbit anti-erb-B4 polyclonal antibody (Santa Cruz) for erb-B2 and erb-B4, respectively. All membrane treatments are as described subsequently for Western-blotting analysis under "Experimental Procedures" except an anti-rabbit IgG HRP conjugate was employed for erb-B4 detection.

Monoclonal Antibody Production and Enzyme-linked Immunosorbent Assay (ELISA) Screening—To generate monoclonal antibodies (mAbs) using recombinant SPGF protein, 8-week-old BALB/c mice were immunized (intraperitoneally) with 50 μ g of SPGF 4–5 times at 2-week intervals. The first immunization was done in Freund's complete adjuvant followed by incomplete Freund's adjuvant for subsequent immunization. Mice were sacrificed 5 days after the final boost, and the cells from splenocytes were fused with NS-1 myeloma cells using a standard fusion protocol (11). Hybridomas were screened by ELISA. Antibody-secreting hybridomas were cloned twice by limiting dilution before

being inoculated into pristane-primed mice for production of ascitic fluid. mAbs were purified using a protein G column. The three mAbs used in this study, 2-22, 11D7, and 13E8, are all of the IgG2b isotype.

ELISA was performed in 96-well plates to which Ni²⁺-nitrilotriacetic acid had been coated (Ni-NTA HisSorb, Qiagen). 50 μ l of SPGF at a concentration of 5 μ g/ml in PBS containing 1% BSA and 0.05% Tween 20 were plated on nickel plates for 5 h at 4 °C followed by washing three times with PBS containing 0.1% BSA and 0.05% Tween 20. 50 μ l of each hybridoma supernatant were added per well and incubated overnight at 4 °C with shaking. After washing 3 times with PBS containing 0.1% BSA and 0.05% Tween 20, 50 μ l of goat anti-mouse IgG (H+L)-horseradish peroxidase conjugate (Bio-Rad) were added for 90 min (1:2000 dilution) in 1% BSA and PBS buffer at 4 °C. Plates were washed twice with 0.1% BSA, 0.05% Tween 20 in PBS buffer and twice with PBS alone and developed with ortho-phenylene diamine as a substrate. The reaction was stopped after 7 min with 2.25 M H₂SO₄. The optical density at 490 nm was measured.

Surface Plasmon Resonance Binding Analyses—All experiments were performed on a BIAcore 3000 instrument (Biacore, Piscataway, NJ) at 25 °C in Hepes-buffered saline running buffer (150 mM NaCl, 3.4 mM EDTA, 0.005% surfactant P-20, 10 mM Hepes, pH 7.4). To test the antigenic reactivity of 2-22, 11D7, and 13E8 antibody to SPGF and VGF, each antibody was coupled to the CM5 chip surface using an amine coupling kit at a flow rate of 5 μ l/min. Then SPGF and VGF at a concentration of 8 μ g/ml were individually passed over each immobilized antibody surface. The sensor surface was regenerated between binding reactions by 2 washes of 10 mM glycine buffer, pH 9.5, for 15 s at 100 μ l/min. For determination of the kinetics of antigen-antibody binding, 2-22 and 13E8 mAbs were individually immobilized on the CM5 chip surface using a standard amine coupling procedure. For each antibody, all experiments were performed on three surfaces of different ligand densities ranging from 1000 to 1500 response units. Association was measured by passing various concentrations of SPGF or VGF (1–10 nM) over each ligand surface for 2 min at a flow rate of 50–100 μ l/min. The sensor surface was regenerated between binding reactions by two washes of 10 mM glycine buffer, pH 9.5, for 15 s at 100 μ l/min. Identical injections over blank surfaces were subtracted from the data to determine specific binding. Binding kinetics were evaluated in a 1:1 binding model (12).

Human Keratinocyte and Fibroblast Mitogen Assays—The normal primary human dermal fibroblast line R2F (13) was cultured in Complete fibroblast medium, consisting of Dulbecco's modified Eagle's medium/F-12 medium (Invitrogen) supplemented with 15% calf serum (Hyclone, Inc.) and 10 ng/ml EGF. The normal primary human epidermal keratinocyte line N (14) was cultured as described (15) in Complete keratinocyte medium consisting of Invitrogen keratinocyte serum-free medium (Invitrogen) supplemented with 30 μ g/ml bovine pituitary extract, 0.2 ng/ml EGF, and 0.3 mM CaCl₂. Mitogenicity assays were performed by plating R2F and N cells at low density in reduced serum and reduced bovine pituitary extract versions of their respective media formulations and without EGF such that their proliferation in response to a range of concentrations of added mitogen could be assessed.

3000 R2F cells were plated in replicate 9-cm² wells in Dulbecco's modified Eagle's medium/F-12 plus 1% calf serum. The next day and also the fourth day after plating, the wells were refed with this medium supplemented with a range of EGF and SPGF concentrations or with complete fibroblast medium. 1000 N cells were plated in replicate 9-cm² wells in Invitrogen keratinocyte serum-free medium plus 15 μ g/ml bovine pituitary extract plus 0.3 mM CaCl₂. The next day and also the fourth day after plating, the wells were refed with this medium supplemented with a range of EGF and SPGF concentrations or with complete keratinocyte medium. The well cultures were trypsinized and counted 6 days after plating. The proliferation rate was measured as population doublings per day: log₂ (number of cells after 6 days/number of cells plated)/6.

SPGF Biotinylation and Binding to Epithelial Cells Analyzed by FACS—SPGF was biotinylated using the ECL protein biotinylation module (Amersham Biosciences) according to the manufacturer's protocol. 1×10^5 MB468 cells (or MB453 cells) were used for each sample. For direct binding assay (Fig. 2D), 1 aliquot of cells was incubated with 1 μ g of anti-EGFR blocking antibody (528, Santa Cruz) at 4 °C for 1 h. Different concentrations of biotinylated SPGF in 50 μ l of FACS buffer (1 \times PBS, 2.5% FCS, 0.02% NaN₃) were added to the various cells and further incubated at 4 °C for 45 min. For competition assays (Fig. 2A), cells were incubated with 50 μ l of FACS buffer containing different amounts of unlabeled SPGF, epiregulin, and EGF at 4 °C for 20 min, then 25 ng of biotinylated SPGF was added to each tube with further incubation at 4 °C for 30 min. Cells were washed in FACS buffer, and

biotinylated SPGF was visualized by streptavidin-phycoerythrin (Molecular Probes) using FACS, recording the mean fluorescence intensity (MFI). Inhibition was plotted as percentage expressed as $(MFI - MFI_{neg}) / (MFI_{max} - MFI_{neg})$.

Cell Lysate Preparation, Immunoprecipitation, and Western Blotting—HeLa cells (80–90% confluent) in 10-cm culture dishes were stimulated with 50 ng/ml ligands at 37 °C for 10 min. The dish was washed once with ice-cold PBS. Cells were directly lysed by 1 ml of lysis buffer (25 mM Tris, pH 7.4, 150 mM NaCl, 1% Triton X-100, 1 mM phenylmethylsulfonyl fluoride, 0.35 trypsin inhibitor units/ml aprotinin, 5 µg/ml leupeptin, 10 mM NaF, 10 mM β-glycerophosphate, and 1 mM Na₃VO₄) at 4 °C for 30 min. After spinning the samples, 0.5 ml of lysate was immunoprecipitated by 1 µg of anti-EGFR (goat polyclonal, Santa Cruz Biotechnology) and 10 µl of GammaBind plus beads at 4 °C overnight. Beads were washed 3 times and eluted directly in 2× SDS-PAGE loading buffer. The total cell lysates and immunoprecipitated samples were resolved by 7.5% SDS-PAGE followed by Western blotting to polyvinylidene difluoride membranes. The membrane was blocked in 2.5% BSA, Tris-buffered saline with Tween (TBST) (for EGFR) or 2% gelatin, TBST (for 4G10) at 37 °C for at least 30 min. Primary antibody was incubated with membranes overnight at 4 °C according to the manufacturer's recommendation. Membranes were washed and incubated with 1:10,000 anti-goat IgG (for EGFR) or anti-mouse IgG2b (for 4G10) HRPO conjugates at room temperature for 1 h. After extensive washing, the membranes were developed using a chemiluminescence reagent kit (PerkinElmer Life Sciences) on MR film (Eastman Kodak Co.).

Affinity of SPGF Binding to EGFR—A lactoperoxidase-catalyzed method was used for labeling SPGF, whereas a chloramine T-catalyzed method was used for EGF. The specific activity of labeled SPGF was 0.54 pmol/cpm, whereas EGF had 0.34 pmol/cpm. MB468 cells were plated at 3×10^4 /0.1 ml/96 wells. ¹²⁵I-Labeled SPGF or EGF was added at different concentrations in 50 µl of binding medium (L15 medium with 0.1% NaN₃) at 4 °C and incubated for 5 h. Supernatants were harvested, and the cells were quickly washed twice with 60 µl of ice-cold binding medium. The supernatant and the washes were then combined. 50 µl of 0.5 N NaOH was added into each well at room temperature for 1 h to lyse the remaining material and further washed once with 60 µl of 0.5 N NaOH. γ-Counting was used to determine the free ligand in the culture supernatant as well as the bound ligand in cell lysates. The affinity, receptor number, and Scatchard plot were calculated.

Antibody Blocking Assay—1 µg of anti-EGFR blocking antibody was added to HeLa cells at 37 °C for 30 min, whereas different amounts of antibody 2-22 were premixed with 1 ng of SPGF or EGF at room temperature for 30 min. 1 ng of SPGF or EGF with or without EGFR or premixed 2-22/SPGF or 2-22/EGF was added to 2×10^5 /ml HeLa cells in 24-well plates at 37 °C for 10 min. After washing twice with ice-cold PBS, HeLa cells were lysed in 100 µl of lysis buffer and analyzed by SDS-PAGE and Western blotting as described above.

Molecular Graphics and Modeling—The molecular model of the D4R (residues 40–90) was derived by homology modeling from the three-dimensional coordinates of mouse EGF (PDB code 1EGF) using the package MODELLER (16). Ribbon representations of the structures were generated using MOLSCRIPT (17) followed by image rendering with RASTER3D (18). The molecular surface of the D4R model was generated using GRASP (19). Colored residues in the D4R surface are the equivalent to those in TGF-α, which were found to interact with the L1 (yellow), L2 (red), or both L1/L2 domains (green) of the erb-B1 receptor in the three-dimensional structure of TGF-α in complex with erb-B1 (Fig. 3). Sequence alignment was made using ClustalW (20) and structural alignment was guided by the structure superimposition program TOP (21) (bioinfo1.mbfys.lu.se/TOP). Mapping of accessibility D4R onto the structural alignment was carried out using the program ESPript (22).

Cells and Viruses—Vaccinia virus strain WR was propagated in L929 cells, whereas viral titer assays were performed in Vero cells as previously described (23, 24). Unpurified vaccinia virus from tissue culture supernatants was used for all animal infections.

Vaccinia Virus Infections—Male, 6–8-week-old C57BL/6 mice (The Jackson Laboratory) were injected intraperitoneally with antibody preparations (200 µg of each antibody) diluted in phosphate-buffered saline except for 2× dosing where 400 µg was used. Six hours later, mice were anesthetized by inhalation of metofane (Pitman-Moore) and were infected intranasally with 1×10^4 pfu of vaccinia virus diluted in 50 µl of medium.

Lung Histological Virus Titration—At the times indicated, one lung from each infected animal was harvested, homogenized in minimum Eagle's medium supplemented with 10% fetal bovine serum, separated

in aliquots, and frozen at –80 °C. The number of pfu/ml in each lung was determined by plaque assay using 10% of the homogenate as previously described (24). The contralateral lung from each VV-infected mouse was collected, fixed in 10% neutral buffered formaldehyde, and then paraffin-embedded. Tissue sections (5 µm) were stained with hematoxylin and eosin and analyzed microscopically under 10× magnification.

Analysis of Adaptive T Cell Response—Single cell suspensions were prepared from spleens, and erythrocytes were removed by lysis using a 0.84% NH₄Cl solution. VV-specific CD8⁺ T cells were detected by measuring IFN-γ secretion to VV-infected fibroblasts (MC57G) using the Cytofix/Cytoperm Kit PlusTM (with GolgiPlugTM, Pharmingen). Briefly, MC57G cells were incubated for 2 h with a 5×10^6 pfu of WR strain of VV (multiplicity of infection 1.2). Subsequently, $1-2 \times 10^6$ splenocytes were incubated in 96-well plates with 2.5×10^5 VV-infected or uninfected MC57G cells in the presence of 10 units/ml human recombinant IL-2 (Pharmingen) and 0.2 µl of GolgiPlugTM for 5 h at 37 °C. After preincubation with 1 µl of Fc BlockTM (2.4G2) in 96-well plates containing 100 µl of FACS buffer (Hanks Balanced Salt Solution, 2% FCS, 0.1% NaN₃), cells were stained (20 min, 4 °C) with combinations of fluorochrome-labeled mAbs specific for CD8α (53-6.7), CD44 (IM7). Subsequent fixation and permeabilization of the cells was performed to allow intracellular access to the anti-IFNγ mAb (XMG1.2; Pharmingen). Freshly stained samples were analyzed using a BD Biosciences FACS-Calibur and CellQuest software (San Diego, CA). Anti-CD3 stimulation was used to detect recently activated CD8⁺ T cells. Splenocytes were incubated with 5 µg/ml purified anti-mouse CD3ε Ab (145-2C11) under the same conditions described above.

Effects of SPGF and Anti-SPGF mAbs on Variola Strain Solaimen Plaque Formation In Vitro—Confluent BSC40 monolayers in two T-162 flasks were infected with variola strain Solaimen at a multiplicity of infection of 0.1. Cells were incubated at 36 °C, 6% CO₂ for 1 h, rocked at 15-min intervals, and overlaid with RPMI supplemented with 2% FBS (RPMI-2%; 35 ml total volume/flask). The virally infected cells were incubated at 36 °C, 6% CO₂ for 72 h. Harvesting of extracellular enveloped virus (EEV) particles was done by pooling the supernatant of the viral infections into a 250-ml centrifuge bottle. Cell monolayers, containing mostly cell associated virus and IMV, were then rinsed with media, scraped into media suspension, pooled into two 50-ml conical tubes, and frozen at –20 °C to be used for future studies.

We estimated that an EEV titer of $\sim 1.5 \times 10^4$ pfu/ml was obtained in the viral infection, and we used this figure to dilute the EEV in RPMI-2% such that we would have 50 pfu/well in the experiment. The diluted EEV was then split into two 50-ml conical tubes. IMV-neutralizing antibody, J2D5 (1:1000), was added to one tube containing diluted EEV particles to neutralize any IMV particles. Diluted virus with or without J2D5 was separated into aliquots and deposited into the 2-ml wells of a 96-well dilution plate. Monoclonal antibodies raised against SPGF (2-22, 2-13, 13E8, and 11D7) were added to each corresponding well at a final concentration of 100 µg. The virus was incubated with or without mAbs at 4 °C for 30 min and subsequently plated onto confluent BSC40 monolayers in 6-well plates. Each mAb was tested in triplicate with or without J2D5. Additionally, we tested the effect of pre-treating the cell monolayer with α-EGFR 528 mAb. Three wells of a 6-well plate were pretreated by adding anti-EGFR mAb (1:1000), whereas the remaining wells were mock-treated with RPMI-2%. The pretreated plate was incubated at room temperature for 30 min before adding diluted virus with or without J2D5. All plates were then incubated at 36 °C, 6% CO₂ for 1 h and rocked at 15-min intervals. The inoculum was removed, and 2 ml of RPMI-2% (with or without J2D5) was added to each well. The plates were incubated at 36 °C, 6% CO₂ for 3.5 days at which time they were stained with 2× crystal violet, and viral plaques were counted. The results in Supplemental Fig. S1 show that mAbs raised against SPGF marginally inhibit viral plaque formation by a population of virus that is predominantly EEV. Because the SPGF is thought to derive from the EEV membrane and EEV particles are the numerically minor fraction of viruses in the population, this experiment shows that anti-SPGF mAbs are not neutralizing mAbs.

To determine whether recombinant SPGF can block variola virus entry into non-transformed human cells, a second type of experiment was performed. Confluent human foreskin fibroblast monolayers in 6-well plates were pretreated with 1 ml of RPMI-2% with and without recombinant SPGF at a concentration of 50 nM 60 min before infection. Cells were then infected at a multiplicity of infection of 5 in 1 ml of total volume with variola strain Solaimen in RPMI-2% with or without 50 nM SPGF. Three wells of each plate were pretreated and infected in the presence of SPGF, and the remaining three wells were mock-treated. The plates were incubated at 36 °C, 6% CO₂ for 1 h and rocked gently

at 15-min intervals to ensure even infection and coverage of the cell monolayer. The inoculum was removed, and 2 ml of RPMI-2% with or without SPGF was added to the appropriate wells. The virally infected cells were incubated at 36 °C, 6% CO₂ and harvested at various times post-infection. An initial time point was harvested when the viral inoculum was removed. Harvesting of time points was done by scraping the cell monolayer from the wells and fully resuspending the viral-infected cells followed by two freeze-thaw cycles. A 100- μ l aliquot of each time point was serially diluted in RPMI-2%. Dilutions 10⁻³–10⁻⁸ were plated on BSC40 confluent monolayers in 6-well plates. Plates were incubated at 36 °C, 6% CO₂ for 1 h and rocked gently at 15-min intervals. The inoculum was removed from each well and 2 ml of RPMI-2% was added. The plates were incubated at 36 °C, 6% CO₂ for 72 h and stained with 2 \times crystal violet. Plaques were counted, and the titer of the virus (pfu/ml) was determined. The results in Supplemental Fig. S2 demonstrate that saturation of erb-B1 sites on human foreskin fibroblasts fails to block variola entry of IMV and EEV components.

RESULTS

Bioinformatic Analysis and Target Selection—Systematic, detailed comparison of the complete variola major genes (India 1967 GI:9627521 (185,578 bp) and Bangladesh GI:623595 (186,103 bp)) and those of variola minor (Alastrim GI:5830555 (186,986 bp)), a less pathogenic variant, reveals 97% overall identity at the nucleotide level (25–27). Likewise, comparison of variola genes with that of VV (Copenhagen GI: 9790357 (191,736 bp)) shows ~95% identity, accounting for smallpox cross-protection from VV immunization. Because relevant targets of joint cellular and humoral immunity require both T and B cell epitopes and necessitate accessibility of antibody to native viral protein, we searched the variola major genome for those genes encoding a signal sequence characteristic of many secreted and integral membrane proteins. Table I lists the 25 candidate genes in the variola major Bangladesh genome whose products include a signal sequence as defined by SIGNALP (28). Using TMHMM (29) and PSORT (30), which identify transmembrane anchors and other predictors of protein localization in eukaryotic cells, respectively, these candidates were divided into two principle groups, type I integral membrane proteins and secreted proteins.

Functional annotation was then accomplished by 1) sequence similarity comparison through BLAST search (31) against NR and Swiss protein databases, 2) structural homology analysis by BLAST search to the PDB data base, and 3) domain structure analysis using SMART (32) and PFAM (33). Type I integral membrane proteins include: D4R, a homologue of human epiregulin (EPI); A46R, C9L, and J7R membrane glycoproteins, the latter being hemagglutinin-like; A41L, a homologue of an integrin-associated protein; B6R, a transmembrane complement control protein with four concatamerized domains, analogous to the soluble D15L molecule. Predicted secreted molecules include: D7L, a candidate IL-18-binding protein; A44L and G3R, orthologues of cowpox-soluble secreted chemokine inhibitors; B8R, structurally related to the extracellular region of human interferon γ receptor; B17R, a structurally related ligand binding domain of the human IL-1 receptor; C2L, a homologue of human plasminogen activation inhibitor.

From this analysis and consistent with other earlier published data (3, 4, 25), it is clear that the variola immune evasion strategy is, in significant part, to block inflammation normally induced by chemokines, cytokines, complement and plasminogen activation. This inflammation blockade permits variola virus to function as a high fidelity replicon without the need to exploit mutational mechanisms to escape immune detection. The variola virus D4R gene product is attractive as an immune system target within the candidate group in several respects. First, this gene encompasses the counterpart of the vaccinia growth factor, an EGF-like ligand that has been involved in the pathogenesis of vaccinia (6). For this reason we shall refer to

the D4R fragment homolog of VGF as SPGF. Second, among orthopox viruses, this 140-amino acid gene product is highly conserved (84–100% amino acid identity) (Fig. 1) yet shares only 30% amino acid identity with epiregulin, its closest human homologue encompassing an EGF domain as well. Thus, the viral product is unlikely to be immunologically cross-reactive with the mammalian growth factor. Epiregulin shares the same structural architecture as the orthopox growth factors (Fig. 1), consisting of a leader sequence, EGF-like ectodomain, transmembrane segment, and short cytoplasmic tail and binds to the erb-B family of epidermal growth factor receptors with differing specificity and biological effect relative to EGF (34, 35). Third, interaction with a variola-derived growth factor might explain the basis of skin lesions in infected humans since primary basal skin keratinocytes constitutively express EGF receptors (36). That VGF was shown to be a pathogenic early gene product through elegant molecular virology studies (6, 37) further underscores the potential importance of this target.

D4R Protein Fragment Expression and Cellular Binding—A high degree of sequence similarity exists within the EGF domain of orthopox virus growth factor family members (Fig. 1). By analogy with native mammalian EGF and VGF, which exist as membrane-associated precursors post-translationally cleaved to liberate soluble factors (38), the D4R protein was expected to be similarly processed. Therefore, we expressed a D4R protein fragment corresponding to SPGF as inclusions in *E. coli* using an N-terminally His-tagged protein incorporating the EGF domain (amino acid residues 40–90), refolded, and purified by high performance liquid chromatography as described (see “Experimental Procedures”). This recombinant DNA expression strategy obviated requirements to accommodate the *N*-linked glycan adduct *N*-terminal to the EGF domain as well as four conserved putative *O*-linked glycan sites, two flanking the *N*-linked site and two proximal to the transmembrane region (Fig. 1). In Fig. 2, panel A, the inset shows a Coomassie-stained 15% SDS-PAGE gel of purified SPGF migrating as an 8-kDa band as compared with recombinant EGF at 6 kDa and EPI at 5 kDa. The relative affinity of these three ligands for human MB468 epithelial cells was tested by flow cytometry in panel A. Cellular binding of the growth factors was assayed using biotinylated-SPGF plus streptavidin-phycoerythrin with prior incubation of varying amounts of unlabeled SPGF, EGF, or EPI. Note that the EGF and SPGF binding inhibition curves are similar, but EPI requires an ~10-fold higher concentration to achieve 50% inhibition. Fig. 2B shows Scatchard analysis of ¹²⁵I-labeled SPGF on MB468 cells. Two receptor classes are defined; they are a high affinity class with a $K_d = 0.14$ nM and 5.5×10^4 sites per cell and a low affinity class with a $K_d = 258$ nM and 8.8×10^6 sites per cell. After binding, SPGF is able to induce proliferation of human keratinocytes (*N*) and fibroblasts (*R2F*), supporting long term cell growth at subnanomolar concentrations, consistent with the functional relevance of the high affinity sites (Fig. 2C). The Fig. 2C inset represents a 4G10 anti-phosphotyrosine Western blot of total cell lysates from unstimulated, SPGF-, EGF-, or EPI-stimulated epithelial cells. Note how the same cellular substrates are phosphorylated for each of the three ligands. SPGF, like EPI and EGF, also induces phosphorylation of the EGFR.

SPGF Binding to erb-B1—There are four subtypes of EGF receptors: erb-B1, erb-B2, erb-B3, and erb-B4. The tumorigenic leporipoxviruses, Shope fibroma virus, and myxoma virus and the cytolytic vaccinia *Orthopoxvirus* all display unique patterns of erb-B receptor kinase interaction relative to each other (10). Whereas the Shope growth factor is a broad specificity ligand, VGF primarily binds erb-B1, and the myxoma virus growth factor binds to erb-B2/erb-B3 heterodimers. To determine

TABLE I
Analysis of variola major genes containing a leader sequence in the Bangladesh strain

Gene (GenBank TM accession no.)	Amino acid	Cleavage ^a	Transmembrane ^b	PDB HIT ^c	Domains ^d (x)	Comments
D4R (438919)	140	20	100–125	1EGF EGF_HUMAN	PF0008: EGF (1)	Homolog of human epi-regulin (GenBank TM accession no. 7438519). Epidermal growth factor.
D7L (438922)	126	17	None	None	None	Homolog of IL-18-binding protein (GenBank TM accession no. 8099344).
D15L (438930)	263	20	None	1G40 VCP_VACCV	PF00084: SCR (4)	Ortholog of vaccinia complement control protein (VCP_VACCV). Homolog of variola B6R.
O2L (438937)	220	18	None	1IAL: A (0.2)	None	PDB hit points to the arm repeat (PF00514) of mouse importin α (GenBank TM accession no. 6754474).
C2L (438940)	373	16	None	1DB2 PAI1_HUMAN	PF00079: Serpin (1)	Member of the serine protease family. Homolog of human plasminogen activator inhibitor (PAI1_HUMAN).
C9L (438947)	348	47	312–334	1DCL: A (0.66)	None	Variola 36-kDa major membrane glycoprotein PDB hit points to the IG domain of GenBank TM accession no. 126559.
A41L (439062)	277	23	125–147, 154–176, 186–208, 215–237, 247–269	None	None	Homolog of integrin-associated protein (GenBank TM accession no. 7208759).
A44L (439065)	218	18	None	1CQ3: A VCCI_COWPOX	PF02250: ORTHOPOX_35kD (1)	Homolog of cowpox-soluble secreted chemokine inhibitor VCCI_COWPOX and variola G3R.
A46R (439067)	195	22	167–189	None	None	Membrane glycoprotein.
J7R (439077)	313	17	278–300	1F3R: B	PF00047: IG (1)	Hemagglutinin antigen, adhesion molecule.
B4L (439082)	85	25	None	None	None	Unknown. This protein is only present in variola.
B6R (439084)	317	20	280–302	1G40 VCP_VACCV	PF00084: SCR (4)	Homolog of D15L and vaccinia complement control protein (VCP_VACCV).
B8R (439086)	266	17	None	1FYH: B INGR_HUMAN	None	Homolog of human interferon γ receptor (INGR_HUMAN). May bind IFN γ .
B17R (439095)	354	23	None	1ITB: B IL1R_HUMAN	PF00047: IG (2)	Homolog of human IL-1 receptor (IL1R_HUMAN). May bind IL-1.
B22R (439100)	1897	19	1834–1856	None	None	Unknown. Contains internal repeats.
G2R (439102)	348	23	None	1TNR: R TNFR1_HUMAN	PF00020: TNFR (3)	Homolog of human TNF receptor 1 (TNFR1_HUMAN). May bind TNF.
G3R (439103)	253	18	None	1CQ3: A VCCI_COWPOX	PF02250: ORTHOPOX_35kD (1)	Ortholog of cowpox-soluble-secreted chemokine inhibitor (VCCI_COWPOX). Homolog of variola A46L.
E5R (438964)	341	27	None	None	None	Unknown
E10R (438969)	95	22	None	None	None	Unknown
K5L (438977)	79	27	49–71	None	None	Unknown
H3L (438982)	111	18	None	None	None	Unknown
A14L (439035)	68	22	None	None	None	Unknown
A15L (439036)	90	30	46–68	None	None	Unknown
A22L (439042)	117	21	None	None	None	Unknown
A31.5L(623596)	146	24	None	None	None	Unknown

^a Cleavage sites of N-terminal signal sequences were predicted using SIGNALP (4). Note that orthopox viruses exist in two major particle forms, the IMV particle and the EEV particle (22).

^b Transmembrane regions were detected using the program TMHMM (23).

^c Sequences were blasted against the PDB database, and the most significant hit is reported here ($e \leq 0.01$) along with the name of the sequence hit in Swiss-prot format (protein_specie). Suboptimal hits ($0.01 < e < 1$) are also reported and will be subject to further analysis. The sequence name is not given for suboptimal hits.

^d Domains were detected using PFAM (9). PFAM domain IDs are indicated, as well as the number of times (x) the domain is found in the protein.

which receptor binds SPGF, two sets of binding experiments were performed with biotinylated SPGF using the MB453 (erb-B1⁺B2⁺B3⁺B4⁺) and MB468 (B1⁺B2⁻B3⁺B4⁻) human epithelial cell lines and flow cytometry. As shown in Fig. 2D, at no concentration of SPGF is binding detected on MB453 cells. By contrast, MB468 cells bind SPGF in a dose-dependent manner, and this binding is readily blocked with the anti-erb-B1-specific mAb 528. These results show that erb-B1 is necessary for SPGF binding. To determine whether erb-B1 alone or in conjunction with erb-B3 is required for SPGF binding, chemical cross-linking of biotinylated SPGF was performed after binding to MB468 cells followed by receptor subtype-specific antibody

immunoprecipitation and Western blotting with streptavidin-HRPO. The Fig. 2D, inset demonstrates that only erb-B1 interacts with SPGF in a detectable manner.

Affinity and Specificity of Anti-SPGF Monoclonal Antibodies—In view of the subnanomolar affinity of SPGF binding to erb-B1, any attempt at blockade of the viral growth factor-cellular receptor interaction and downstream signaling requires a high affinity antibody. To this end, we developed mAbs in Balb/c mice to SPGF first by screening for ELISA reactivity against the immunizing SPGF, then testing those reactive antibodies for their ability to inhibit biotinylated-SPGF binding to erb-B1-expressing epithelial cells and subsequently determin-

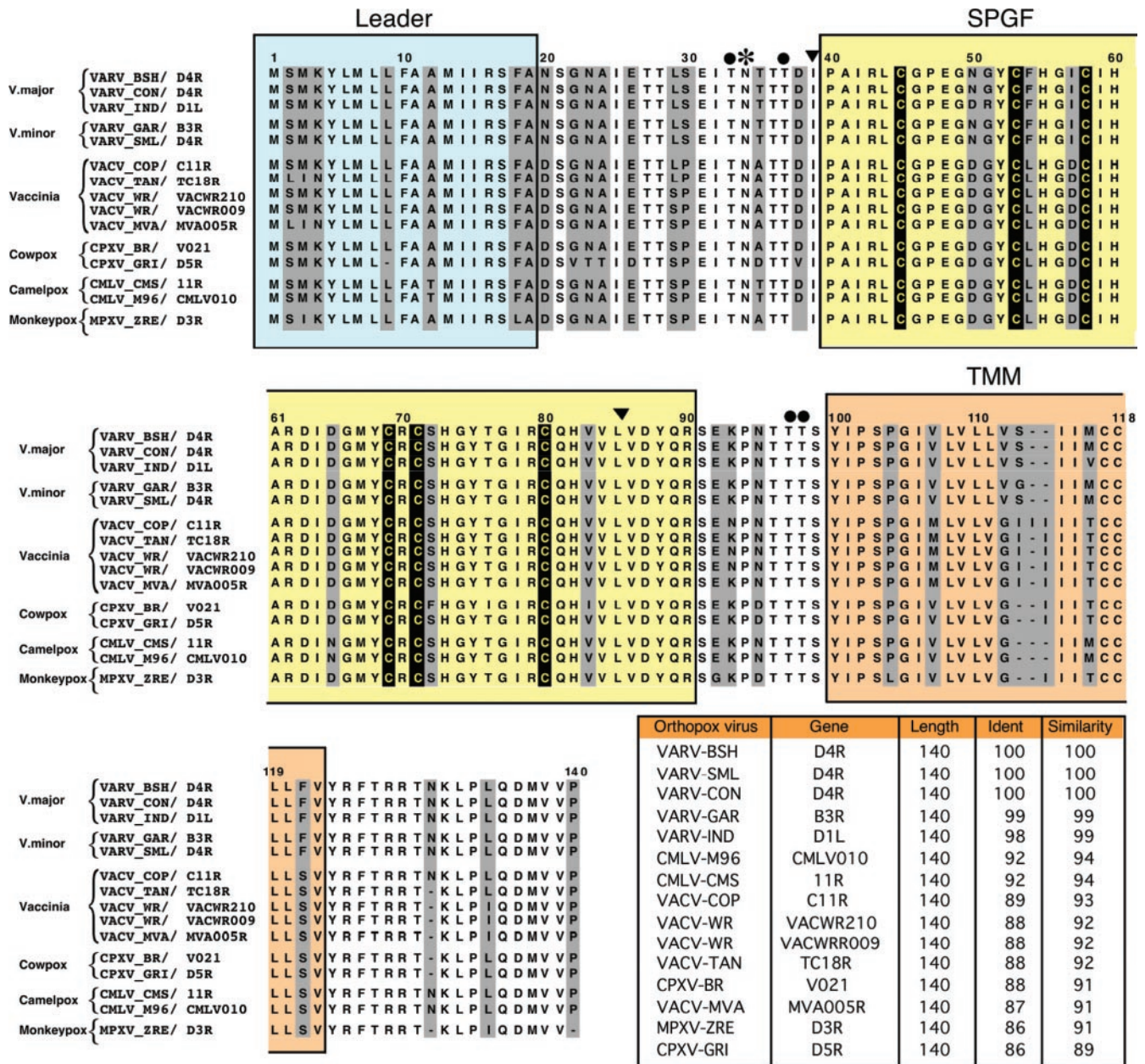


FIG. 1. Conservation of epiregulin-like growth factors among orthopox viruses. Examples of orthopox virus growth factor sequences for variola major, variola minor, vaccinia, cowpox, camelpox, and monkeypox viruses are shown in the single-letter amino acid code. The orthopox virus strain and gene name, encoded protein length, and identity/similarity to variola Bangladesh are given. The predicted leader sequence, EGF domain, and transmembrane region are shaded in blue, yellow, and orange, respectively. The six cysteine residues that form three sets of disulfide bonds characteristic of EGF domains are highlighted in black. The potential N-linked glycosylation site (www.cbs.dtu.dk/services/NetNGlyc) and O-linked glycosylation sites (53) are denoted by the solid star and circles, respectively. The two solid triangles demarcate the mature human epiregulin boundaries (39). Alignment was made using ClustalW (20). Residues shaded in gray signify the only variable positions in the analysis of these sequences. TMM, transmembrane segment.

ing the affinity of blocking mAbs by BIAcore. Surprisingly, antibodies directed against the N-terminal linker proximal to the EGF domain all augmented SPGF binding to erb-B1-expressing cells (data not shown). This effect may result from reduced SPGF tumbling rates in solution, essentially pre-configuring the interaction surface of SPGF for erb-B1 binding. In contrast, antibodies directed at the EGF domain blocked cellular binding. Kinetic analysis (Fig. 3, A and B) for two representative antibodies of the blocking type, 2-22 and 13E8, shows a 20-fold difference in the affinity for SPGF, primarily as a result of the enhanced 2-22 off-rate.

The mAb specificity for other orthopox virus growth factors was assessed on VGF (Copenhagen) produced and purified in a manner identical to SPGF. 2-22 fails to bind to VGF (data not

shown), whereas 13E8 shows binding to VGF but with activity reduced 10-fold relative to SPGF (Fig. 3, A and B). Because the recombinant SPGF and VGF proteins differ at only 3 of 51 residues within the EGF domain, two residues predicted to lie within the β 1- β 2 loop and one residue predicted in the β 2 strand by structure-based alignment, one or more of these residues directly or indirectly reduces 13E8 mAb affinity (Fig. 3C). Based on homology modeling using the recent structure of TGF- α -erb-B1 and EGF-erb-B1 co-complexes (40, 41) (Fig. 3D), the non-conservative I18D mutation may readily influence mAb binding without involving EGFR contacts. Importantly, 2-22 specifically blocks SPGF- but not EGF-induced tyrosine kinase activity of epithelial cells (Fig. 3E), thus being specific for the viral protein. Such inhibition requires a 1000-fold molar

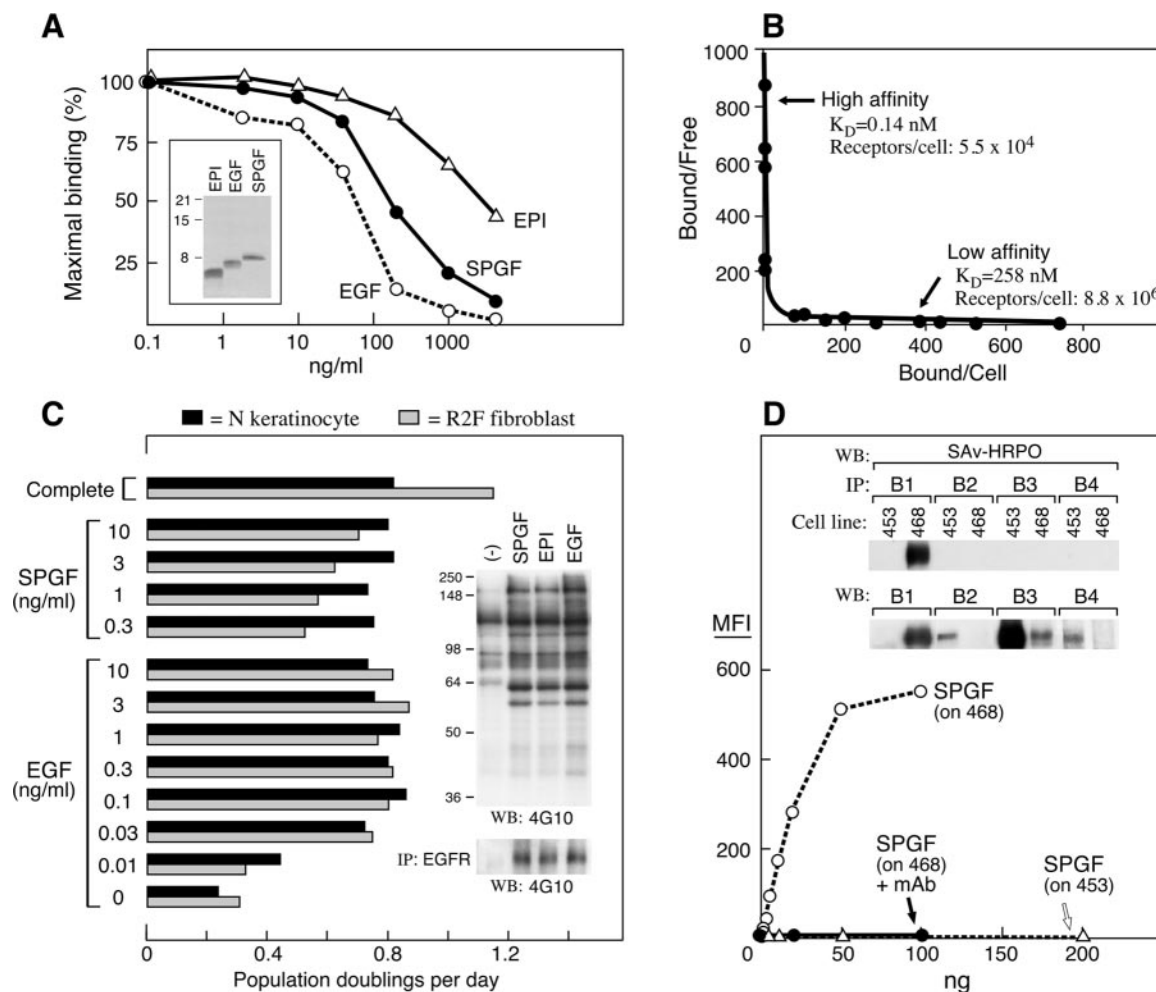


FIG. 2. Interaction of SPGF with human epithelial cells; binding and functional analyses. A, relative ligand affinity for EGF receptors. Unlabeled ligands at indicated concentrations (*abscissa*) were incubated with cells followed by the addition of 250 ng of biotinylated SPGF to compete with “cold” ligands. The bound biotinylated SPGF was visualized by streptavidin-phycoerythrin, and the percentage of maximal binding (*i.e.* in the absence of cold competition) was calculated (*ordinate*) from the mean fluorescence intensity of the FACS analysis. The *inset* shows a Coomassie-stained 15% SDS-PAGE of 5 μ g of SPGF, mammalian epiregulin (34) and human EGF (Sigma). B, Scatchard analysis of SPGF binding to MB468 cells. 125 I-labeled SPGF was used, and binding affinity and receptor numbers were determined (as described under “Experimental Procedures”). C, relative mitogenicity of EGF and SPGF for normal human dermal fibroblasts and epidermal keratinocytes. Proliferation was measured as population doublings per day over a 6-day interval. Replicate cultures were performed that did not vary more than 10%. The *inset* shows Western blotting of total HeLa cell lysates (*upper panel*) and EGFR immunoprecipitation (*lower panel*) using 4G10 anti-phosphotyrosine-specific mAb. D, SPGF binding specificity for erb-B1. MB453 and MB468 cell lines were incubated with biotinylated SPGF in the presence or absence of anti-erb-B1 blocking antibody followed by streptavidin-phycoerythrin, staining and FACS analysis. The MFI number represents mean fluorescence intensity of fluorochrome staining. *Inset*, Western blotting of EGFR subtype-specific immunoprecipitates (B1, B2, B3, and B4) after 1) biotinylated SPGF binding to MB453 and MB468 plus chemical cross-linking, developed with streptavidin-HRPO, and 2) parallel probing with receptor subtype-specific polyclonal antibodies. IP, immunoprecipitates; WB, Western blot.

excess of antibody over SPGF. Similar results were observed with 13E8 and 11D7, two other mAbs that cross-block 2-22 (data not shown). Collectively, the data reveal two features of antibody reactivity against orthopox growth factor proteins. 1) Cross-reactivity between closely related gene orthologues is not assured, and 2) high affinity interaction (such as occurs between erb-B1 and SPGF) requires appropriate mAb affinity, molarity, and specificity to block a pathogenic factor effects on host cells.

In Vivo Murine Model Protection Analysis—Given the ability of 11D7 and 13E8 mAbs to bind VGF, we assessed the protective effects of their parenteral administration in a VV-induced pneumonia model in mice (42). To this end, a LD_{50} (1×10^4 pfu) of vaccinia virus (WR) was given intranasally 6 h after a single intraperitoneal injection with 200 μ g of 11D7, 13E8, or an irrelevant negative control mAb (1A3). As a positive control, a known neutralizing mAb (7D11) against the IMV particle protein L1R was administered (43). Fig. 4A shows the results of representative experiments when mice were analyzed 7 days

post-infection. Although the neutralizing antigen L1R mAb reduced the viral titer of pfu in lung by ~ 100 -fold, the anti-SPGF mAbs 11D7 or 13E8 were without effect. These data suggest that orthopox virus growth factor is not a neutralization target, as further confirmed by *in vitro* analysis (Figs. S1 and S2). Consequently, we performed a second set of experiments using either the L1R-specific mAb alone or in combination with 13E8. We reasoned that inhibition of viral translocation into cells by anti-L1R would retard initial IMV replication. Because IMV entry is facilitated by actin and ezrin protrusions stimulated by protein phosphorylation (44) and growth factor-triggered cellular activation enhances viral replication and subsequent viral particle release from cells, blockade of erb-B1 interaction with VGF/SPGF could further limit viral infectivity. We, therefore, treated mice with control 1A3 mAb, anti-SPGF 13E8 alone, anti-L1R alone, or anti-SPGF 13E8 and anti-L1R mAbs together and examined intranasally infected mice for lung viral titers on days 4, 6, and 8 post-infection. Fig. 4B shows that the protective effect of anti-L1R alone was

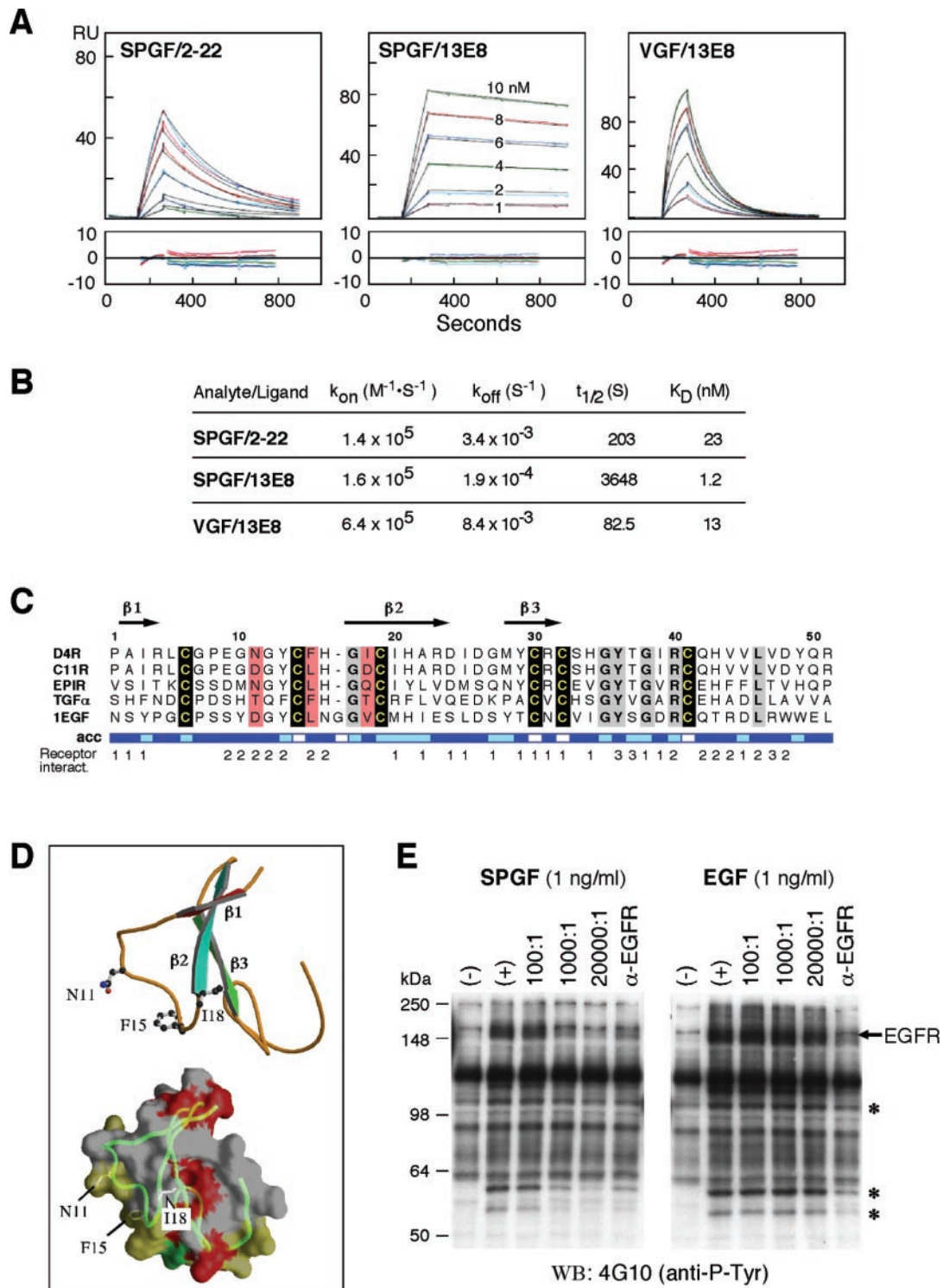


FIG. 3. High affinity mAbs block SPGF-triggered cellular activation. *A*, analysis by surface plasmon resonance of virus growth factor interaction with 2-22 and 13E8 mAbs. Binding sensorgrams at different orthopox virus growth factor concentrations in analyte are indicated, and 1:1 binding model-predicted (*black*) and experimental (*colored*) curves are given for each. Residual values are shown *below* the sensorgrams. *B*, kinetic parameters calculated from BIACore analysis. *C*, structure-based sequence alignment of EGF and TGF- α with epiregulin (*EPIR*), SPGF (*D4R*), and VGF (*C11R*). The position of β 1- β 3 strands in EGF and TGF- α are shown, and surface accessible residues (scale *dark blue*, *light blue*, and *white*, corresponding to high, medium, and low accessibility (*acc*)). *Numbers 1 and 2* refer to ligand binding domains L1 and L2 of EGFR in the TGF- α -EGFR complex (40). *Number 3* denotes a residue interacting with L1 plus L2. Residues *highlighted in red* denote the three amino acids that differ between D4R and C11R. *D*, molecular homology model of SPGF. The *top figure* is a MOLSCRIPT (17) rendition of SPGF with the side chains of the three residues in D4R differing from VGF (C11R) shown. The *bottom figure* offers a GRASP (19) rendition of SPGF also including the predicted residues that contact EGFR L1 domain in *red*, EGFR L2 domain in *yellow*, and both L1/L2 contacts in *green*. *E*, blocking mAbs specifically inhibit SPGF binding and activation of human epithelial cells. 2-22 mAb is preincubated with SPGF (*left panel*) or EGF (*right panel*) then added to HeLa cells. Cell lysates were analyzed by Western blotting (WB) with 4G10. The sample (-) represents no ligand addition, whereas the (+) sample represents the addition in the absence of mAb. *Numbers* indicate the molar ratio of antibody to ligand. Anti-EGFR denotes cell pre-block by the erb-B1 specific mAb 528.

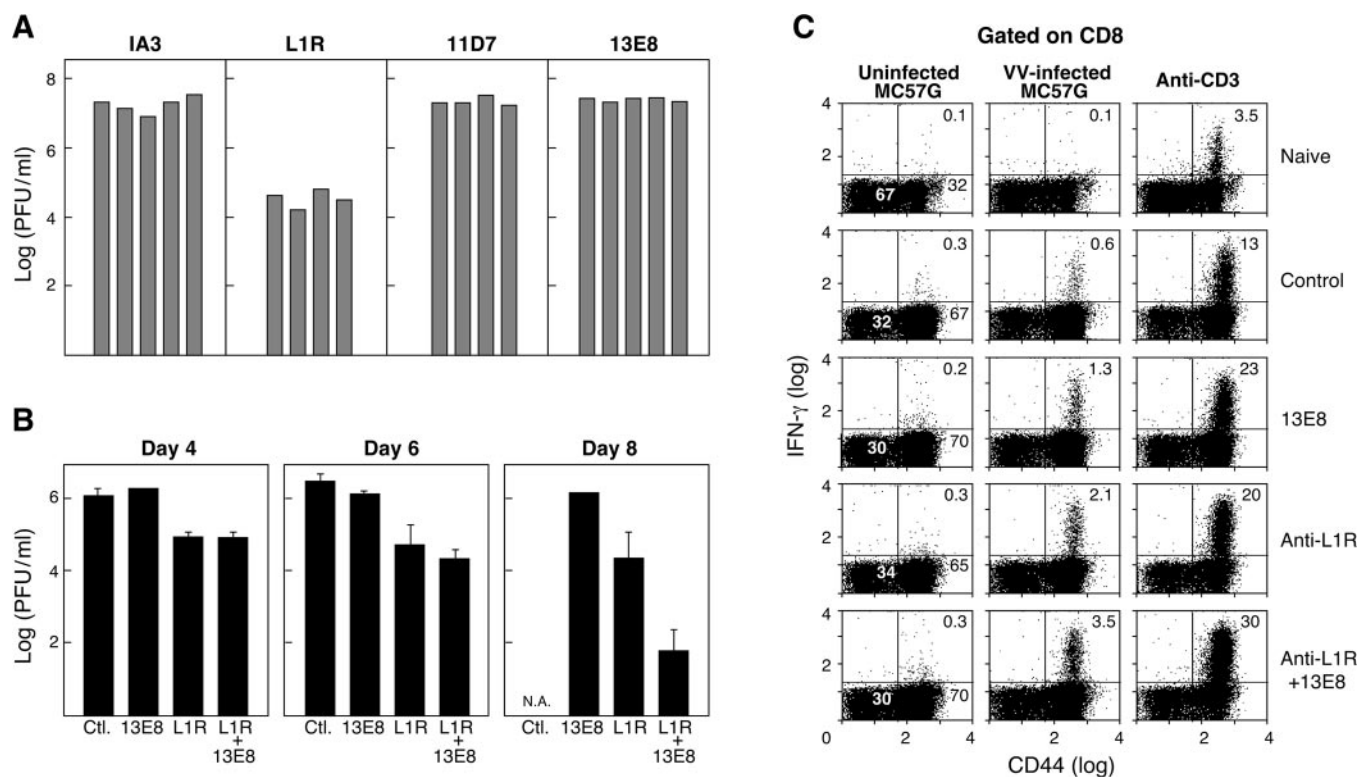


FIG. 4. Anti-SPGF/VGF mAbs modify murine vaccinia infection *in vivo*. *A*, viral titers in lungs of individual male mice after single mAb treatment. Values are those of individual animals. All animals were treated with 200 μ g of each mAb administered intraperitoneally 6 h before intranasal infection with 1×10^4 pfu of vaccinia virus WR. 1A3 is an irrelevant, control mAb. Lungs were harvested on day 7, post-infection. Only anti-L1R treatment (denoted *L1R*) reduced viral titers significantly ($p < 0.0001$ using one-way analysis of variant). *B*, kinetic analysis of plaques in VV-infected animals at days 4, 6, and 8. Treatments with 1A3 (control (*Ctl.*)), 13E8, anti-L1R, or anti-L1R plus 13E8 are shown. Each treatment group consisted of three animals, with the mean and S.D. values noted. At day 8, all three control (1A3) mice had died, and $\frac{2}{3}$ of the 13E8-treated animals had died. *C*, augmentation of adaptive T cell immunity with mAb therapy. Multiparameter flow cytometry analysis of intracellular IFN γ and CD44 expression in splenic CD8 T cells from naive mice or infected untreated mice (control) or infected and treated groups are shown. *In vitro* stimulation of *in vivo* activated T cells is mediated by VV-infected MC57G antigen-presenting cells or anti-CD3 mAb. As a control, results using uninfected MC57G cells are shown. Kruskal-Wallis statistical analysis of control *versus* treated animals for antigen-specific and anti-CD3 stimulated T cells showed $p = 0.038$ and 0.042, respectively.

manifested as early as day 4 and continued through day 8, at which time all the control mice had died. Co-administration of anti-SPGF 13E8 plus anti-L1R had little additional effect through 6 days of post-infection but contributed to a much greater viral clearance between days 6 and 8. This enhanced clearance by the antibody combination was consistently seen in four experiments, with differences of ~ 10 -fold at day 7 and 100–1000-fold at day 8. A control 1A3 mAb plus anti-L1R pair had no such effect (data not shown). Thus, this non-neutralizing mAb to VGF/SPGF augments protective immunity late in infection.

If the mAb pair were protecting exclusively by direct inhibition of viral replication or viral entry, then the reduced viral growth should have been evident in the earlier time periods. Given that VV is controlled by IFN γ -producing T cells, which peak between days 6 and 8 post-infection (45), the kinetics of virus reduction suggest that adaptive immunity is involved. We therefore examined the T cell response in day 7 VV-infected mice treated with control 1A3 mAb, anti-SPGF 13E8, anti-L1R, and the combined anti-SPGF 13E8 plus anti-L1R mAbs. We examined intracellular IFN γ levels in freshly isolated spleen T cells stimulated *in vitro* for 5 h with VV-infected syngeneic MC57G target cells as specific stimulators or with anti-CD3 mAb, which will stimulate all recently activated T cells. The experiments showed increasing IFN γ responses in the CD44⁺CD8⁺ T cells in the VV-infected treatment groups compared with naive uninfected mice in the order 1A3 (control), anti-SPGF 13E8, anti-L1R, and anti-L1R and anti-SPGF 13E8 (Fig. 4C). In this and other experiments, the spleens were

enlarged in the anti-L1R and the anti-L1R plus anti-SPGF 13E8 groups such that, for instance, the total number of VV-specific IFN γ -producing cells per spleen in combined anti-L1R plus anti-SPGF 13E8-treated mice was 11-fold higher than the 1A3-treated mice ($3.3 \pm 1.4 \times 10^5$ *versus* $0.3 \pm 0.1 \times 10^5$, $n = 3$ per group).

The enhanced level of activated IFN γ -producing CD44⁺CD8⁺ splenic T cells in anti-L1R plus anti-SPGF 13E8 mAb-treated mice suggested a reservoir of cells with the potential to migrate to the lung to combat pulmonary infection. Note that CD44, an activation marker up-regulated upon T cell stimulation, is a recyclable receptor for hyaluronan, involved in leukocyte homing to sites of inflammation (46). To test this possibility, lungs were collected from uninfected or from day 7-infected and mAb-treated mice and examined by hematoxylin and eosin staining in tissue sections. As shown in Fig. 5, compared with uninfected mice, where the alveolar spaces are readily evident and bronchiolar epithelium intact, the infected control mAb-treated lungs are characterized by necrotic bronchiolar epithelia and severe alveolar edema, reflected by the weight of the VV-infected lung, about twice that of uninfected lung (0.35 ± 0.04 *versus* 0.21 ± 0.01 g, $n = 3$). The alveolar spaces are obliterated, in fact filled with eosinophilic material and accompanied by few, if any, parenchymal cellular infiltrates. The degree of cellular infiltration increases somewhat in mAb 13E8-treated mice, more so in anti-L1R mAb-treated mice and most dramatically in the combined mAb-treated mice. In the double mAb-treated group, the alveolar spaces are open, and bronchiolar epithelia appear normal. This cellular infil-

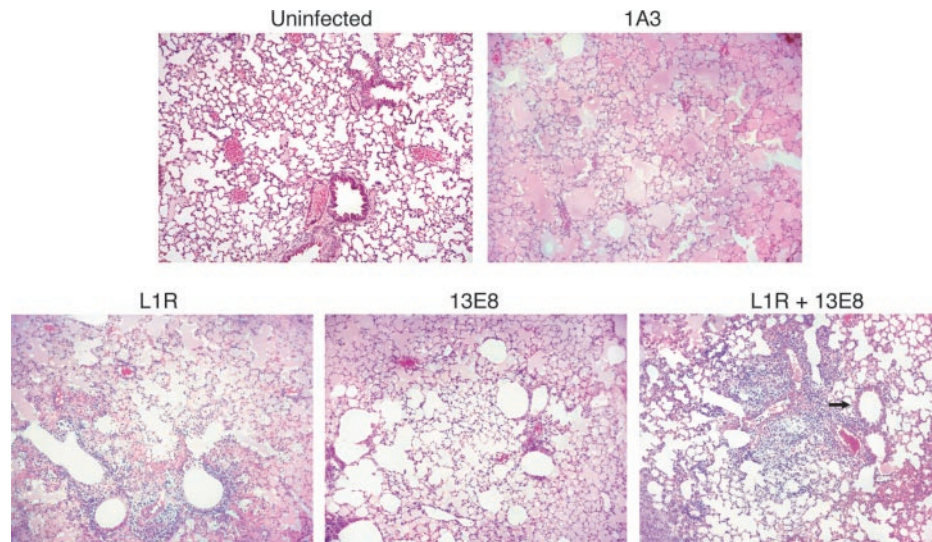


FIG. 5. **Qualitative and quantitative alterations in pulmonary infiltrates by protective mAbs.** Representative hematoxylin and eosin sections ($10\times$ magnification) are shown for lungs from uninfected and infected mice. Pink staining material filling the alveolar spaces in the infected lung represents edema associated with a proteinaceous exudate. The arrow in the anti-L1R plus anti-SPGF 13E8 double mAb treatment group refers to the upper of two bronchioles where the epithelial layer is preserved. Results are representative of a minimum of 10 microscopic fields, examined per slide.

trate is attributable to CD8 T cells in large part. Leukocytes isolated from the pooled lungs of three mAb anti-L1R-treated mice were 25% CD8 and 5% CD4, whereas those isolated from anti-L1R plus anti-SPGF 13E8-treated mice were 34% CD8 and 8% CD4 T cells. Thus, the non-neutralizing anti-SPGF 13E8 mAb enhances clearance of VV in association with augmented T cell responses in the spleen and lung.

DISCUSSION

In the present study, we used genome-wide bioinformatics to identify candidate variola major gene products as potential targets for immune protection. Of these products, D4R was investigated in detail given that EGF-like growth factors are carried by other poxviruses to facilitate viral pathogenesis (Fig. 2 and Refs. 6, 10, and 47). A subnanomolar affinity of interaction between the recombinant SPGF fragment and erb-B1 was noted in the absence of detectable binding to the other members of the erb-B family. Using ELISA screening methods in conjunction with BIAcore binding studies, we identified several mAbs with specificity for SPGF with or without VGF cross-reactivity. These mAbs blocked SPGF-induced tyrosine phosphorylation of erb-B1 and other mammalian cellular substrates without affecting EGF-mediated signaling through the same erb-B1 pathway, consistent with the selective monoclonal antibody specificity for the viral growth factor. Our *in vitro* plaque assay data in the presence of SPGF or its blocking antibodies (Figs. S1 and S2) exclude the possibility that smallpox virus utilizes D4R attachment to EGFR as a primary means to enter mammalian cells and are consistent with the VGF deletion mutant result in the vaccinia system (6). In conjunction with an anti-L1R mAb directed at the IMV (43), anti-SPGF/VGF mAbs afforded immunoprotection in a vaccinia pneumonia model. Importantly, disruption of pathogenic factor-host cell interaction by passive mAb administration is associated with an enhanced T cell immunity. Aside from revealing an unexpected basis for protection and identifying a key orthopox viral target, our findings suggest a strategy for pathogenic factor blockade that may have general utility.

The systemic inflammatory component of innate immunity, the so-called acute phase response, is rapidly induced when organism integrity is breached (48). Sentinel cells including epithelial cells produce IL- 1β and/or IL-6 during this process (49). Blockade of erb-B1 stimulation by the anti-SPGF 13E8

mAb may help avoid subsequent cytokine dysregulation (50, 51). Note that EGF and TGF- α , two erb-B ligands, can induce effusions *in vivo* (52). Orthopox virus growth factors may contribute to an analogous pathology so that 13E8 mAb may be ameliorating in this regard as well.

The present study identifies anti-viral therapeutic mAbs distinct from those mediating viral neutralization. Antibodies in this class afford protection not by blocking viral attachment, fusion, and/or entry *per se* (Figs. S1 and S2) but by inhibiting the action of virus-derived pathogenic factors, *i.e.* inhibiting the viral interference. By extension, inhibition of signaling pathways directed by those factors may also be advantageous to the host. In the case of orthopox viruses, multiple viral proteins that block adaptive and innate immunity are antibody-accessible targets (Table I). Immune modulating antibodies against one or more of these products may shift the balance from viral replication and viral-induced pathology in favor of productive host adaptive immunity. We suspect that targeting of soluble viral decoy receptors and viral factors interfering with host chemokines, cytokines, complement, and plasminogen activation will offer future anti-viral therapeutic strategies.

Anti-orthopox virus growth factor antibody specificities are not detectable in pooled hyperimmune globulin (vaccinia immune globulin) after human vaccinia immunization (data not shown). Likely, the rapid internalization of SPGF/VGF through erb-B1 precludes natural development of antibodies against this viral product. Hence, more protective targets may exist than suggested by host immune responses naturally elicited during the course of infection. The combination of a neutralizing mAb plus such a protective mAb may be particularly advantageous and may represent a treatment for complications of vaccinia immunization or an alternative form of human post-exposure therapy in the event of variola bioattack.

Acknowledgments—We thank Dr. Alan Schmaljohn and United States Army Medical Research Institute of Infectious Diseases, Frederick, MD for providing 7D11 mAb. We thank Dr. Yosef Yarden for providing recombinant epiregulin for this analysis, Dr. Abba Zubair for assistance with statistical analysis, Dr. Kendall Smith for suggestions on Scatchard binding assays, and Drs. Raphael Dolin, Jerome Ritz, and Elliott Kieff for a careful review of the manuscript. We thank the Cell Culture Core of the Harvard Skin Disease Research Center for assistance with the keratinocyte and fibroblast growth assays and Keith A. Daniels for technical support with animal studies.

REFERENCES

1. Fenner, F., Henderson, D. A., Arita, I., Jezek, J., and Ladnyi, I. D. (1988) *Small Pox and Its Eradication*, World Health Organization, Geneva
2. Kempe, C. H. (1960) *Pediatrics* **26**, 176–189
3. Alcamí, A. (2003) *Nat. Rev. Immunol.* **3**, 36–50
4. Seet, B. T., Johnston, J. B., Brunette, C. R., Barrett, J. W., Everett, H., Cameron, C., Spypula, J., Nazarian, S. H., Lucas, A., and McFadden, G. (2003) *Ann. Rev. Immunol.* **21**, 377–423
5. Twardzik, D. R., Brown, J. P., Ranchalis, J. E., Todaro, G. J., and Moss, B. (1985) *Proc. Natl. Acad. Sci. U. S. A.* **82**, 5300–5304
6. Buller, R. M., Chakrabarti, S., Cooper, J. A., Twardzik, D. R., and Moss, B. (1988) *J. Virol.* **62**, 866–874
7. Buller, R. M., Chakrabarti, S., Moss, B., and Fredrickson, T. (1988) *Virol.* **164**, 182–192
8. Apella, E., Weber, I. T., and Blasi, F. (1988) *FEBS Lett.* **231**, 1–4
9. Yarden, Y., and Sliwkowski, M. X. (2001) *Nat. Rev. Mol. Cell Biol.* **2**, 127–137
10. Tzahar, E., Moyer, J. D., Waterman, H., Barbacci, E. G., Bao, J., Levkowitz, G., Shelly, M., Strano, S., Pinkas-Kramarski, R., Pierce, J. H., Andrews, G. C., and Yarden, Y. (1998) *EMBO J.* **17**, 5948–5963
11. Kohler, G., and Milstein, C. (1975) *Nature* **256**, 495–497
12. Kim, M., Chen, B., Hussey, R. E., Chishti, Y., Montefiori, D., Hoxie, J. A., Byron, O., Campbell, G., Harrison, S. C., and Reinherz, E. L. (2001) *J. Biol. Chem.* **276**, 42667–42676
13. Tubo, R. A., and Rheinwald, J. G. (1987) *Oncogene Res.* **1**, 407–421
14. Schön, M., and Rheinwald, J. G. (1996) *J. Investig. Dermatol.* **107**, 428–438
15. Rheinwald, J. G., Hahn, W. C., Ramsey, M. R., Wu, J. Y., Guo, Z., Tsao, H., DeLuca, M., Catricala, C., and O'Toole, K. M. (2002) *Mol. Cell. Biol.* **22**, 5157–5172
16. Sali, A., and Blundell, T. L. (1993) *J. Mol. Biol.* **234**, 779–815
17. Kraulis, P. (1991) *J. Appl. Crystallogr.* **24**, 924–950
18. Merritt, E. A., and Murphy, M. E. P. (1994) *Acta Crystallogr. Sect. D* **50**, 869–873
19. Nicholls, A., Sharp, K. A., and Honig, B. (1991) *Proteins Struct. Funct. Genet.* **11**, 281–296
20. Thompson, J. D., Higgins, D. G., and Gibson, T. J. (1994) *Nucleic Acids Res.* **2**, 4673–4680
21. Lu, G. (2000) *J. Appl. Crystallogr.* **33**, 176–183
22. Gouet, P., Courcelle, E., Stuart, D. I., and Metz, F. (1999) *Bioinformatics* **15**, 305–308
23. Selin, L. K., Nahill, S. R., and Welsh, R. M. (1994) *J. Exp. Med.* **179**, 1933–1943
24. Selin, L. K., Varga, S. M., Wong, I. C., and Welsh, R. M. (1998) *J. Exp. Med.* **188**, 1705–1715
25. Massung, R. F., Liu, L., Qi, J., Knight, J. C., Yuran, T. E., Kerlavage, A. R., Parsons, J. M., Venter, J. C., and Esposito, J. J. (1994) *Virology* **201**, 215–240
26. Shchelkunov, S. N., Massung, R. F., and Esposito, J. J. (1995) *Virus Res.* **36**, 107–118
27. Shchelkunov, S. N., Totmenin, A. V., Loparev, V. N., Safronov, P. F., Gutorov, V. V., Chizhikov, V. E., Knight, J. C., Parsons, J. M., Massung, R. F., and Esposito, J. J. (2000) *Virology* **266**, 361–386
28. Nielsen, H., Engelbrecht, J., Brunak, S., and von Heijne, G. (1997) *Int. J. Neural Syst.* **8**, 581–599
29. Sonnhammer, E. L., von Heijne, G., and Krogh, A. (1998) in *Sixth International Conference on Intelligent Systems for Molecular Biology* (Glasgow, J., Littlejohn, T., Major, F., Lathrop, R., Sankoff, D., and Sensen, C., eds) pp. 175–182, AAAI Press, Menlo Park, CA
30. Nakai, K., and Kanehisa, M. (1992) *Genomics* **14**, 897–911
31. Altschul, S. F., Madden, T. L., Schaffer, A. A., Zhang, Z., Miller, W., and Lipman, D. J. (1997) *Nucleic Acids Res.* **25**, 3389–3402
32. Schultz, J., Copley, R. R., Doerks, T., Ponting, C. P., and Bork, P. (2000) *Nucleic Acids Res.* **28**, 231–234
33. Bateman, A., Birney, E., Durbin, R., Eddy, S. R., Howe, K. L., and Sonnhammer, E. L. (2000) *Nucleic Acids Res.* **28**, 263–266
34. Shelly, M., Pinkas-Kramarski, R., Guarino, B. C., Waterman, H., Wang, L.-M., Lyass, L., Alimandi, M., Kuo, A., Bacus, S. S., Pierce, J. H., Andrews, G. C., and Yarden, Y. (1998) *J. Biol. Chem.* **273**, 10496–10505
35. Komurasaki, T., Toyoda, H., Uchida, D., and Morimoto, S. (1997) *Oncogene* **15**, 2841–2848
36. Nanney, L. B., Stoscheck, C. M., King Jr., L. E., Underwood, R. A., and Holbrook, K. A. (1990) *J. Investig. Dermatol.* **94**, 742–748
37. Stroobant, P., Rice, A. P., Gullick, W. J., Cheng, D. J., Kerr, I. M., and Waterfield, M. D. (1985) *Cell* **42**, 383–393
38. Brown, J. P., Twardzik, D. R., Marquardt, H., and Todaro, G. J. (1985) *Nature* **313**, 491–492
39. Toyoda, H., Komurasaki, T., Uchida, D., and Morimoto, S. (1997) *Biochem. J.* **326**, 69–75
40. Garrett, T. P. J., McKern, N. M., Lou, M., Elleman, T. C., Adams, T. E., Lovrecz, G. O., Zhu, H.-J., Walker, F., Frenkel, M. J., Hyne, P. A., Jorissen, R. N., Nice, E. C., Burgess, A. W., and Ward, C. W. (2002) *Cell* **110**, 763–773
41. Ogiso, H., Ishitani, R., Nureki, O., Fukai, S., Yamanaka, M., Kim, J.-H., Saito, K., Sakamoto, A., Inoie, M., Shirouzu, M., and Yokoyama, S. (2002) *Cell* **110**, 775–787
42. Chen, H. D., Fraire, A. E., Joris, I., Brehm, M. A., Welsh, R. M., and Selin, L. K. (2001) *Nat. Immunol.* **2**, 1067–1076
43. Hooper, J. W., Custer, D. M., Schmaljohn, C. S., and Schmaljohn, A. L. (2000) *Virology* **266**, 329–339
44. Locker, J. K., Kuehn, A., Schleich, S., Rutter, G., Hohenberg, H., Wepf, R., and Griffiths, G. (2000) *Mol. Biol. Cell* **11**, 2497–2511
45. Ruby, J., and Ramshaw, I. (1991) *Lymphokine Cytokine Res.* **10**, 353–358
46. DeGrendele, H. C., Estess, P., and Siegelman, M. H. (1997) *Science* **278**, 672–675
47. Opgenorth, A., Nation, N., Graham, K., and McFadden, G. (1993) *Virol.* **192**, 701–709
48. Yoo, J.-Y., and Desiderio, S. (2003) *Proc. Natl. Acad. Sci. U. S. A.* **100**, 1157–1162
49. Schluns, K. S., Cook, J. E., and Le, P. T. (1997) *J. Immunol.* **1158**, 2704–2712
50. Diehl, S., and Rincon, M. (2002) *Mol. Immunol.* **39**, 531–536
51. Tanaka, T., Kanda, T., McManus, B. M., Kanai, H., Akiyama, H., Sekiguchi, K., Yokoyama, T., and Kurabayashi, M. (2001) *J. Mol. Cell. Cardiol.* **33**, 1627–1635
52. Ohmura, E., Tsushima, T., Kamiya, Y., Okada, M., Onoda, N., Shizume, K., and Demura, H. (1990) *Cancer Res.* **50**, 4915–4917
53. Hansen, J. E., Lund, O., Engelbrecht, J., Bohr, H., Nielsen, J. O., Hansen, J.-E. S., and Brunak, S. (1995) *Biochem. J.* **308**, 801–813